Carbon nanofoam supercapacitor electrodes with enhanced performance using a water-transfer process

Article (Published Version)

ACS OMEGA

Article

Cite This: ACS Omega 2018, 3, 15134−15139

http://pubs.acs.org/journal/acsodf

Carbon Nanofoam Supercapacitor Electrodes with Enhanced Performance Using a Water-Transfer Process

Sebastian Nufer,*[,†,‡] Peter Lynch,[‡] Maria Cann,[†] Matthew J. Large,[‡] Jonathan P. Salvage,[§] Sandra Víctor-Román,[∥] Javier Hernández-Ferrer,[∥] Ana M. Benito,[∥] Wolfgang K. Maser,[∥] Adam Brunton,[†] and Alan B. Dalton*[,‡]

[†]M-Solv Ltd, Oxonian Park, Langford Locks, Kidlington, Oxford OX5 1FP, U.K.

[‡]Department of Physics and Astronomy, University of Sussex, Brighton BN1 9RH, U.K.

[§]School of Pharmacy and Biomolecular Science, University of Brighton, Brighton BN2 4GJ, U.K.

[∥]Instituto de Carboquimica (ICB-CSIC), Zaragoza E-50018, Spain

ABSTRACT: Carbon nanofoam (CNF) is a highly porous, amorphous carbon nanomaterial that can be produced through the interaction of a high-fluence laser and a carbon-based target material. The morphology and electrical properties of CNF make it an ideal candidate for supercapacitor applications. In this paper, we prepare and characterize CNF supercapacitor electrodes through two different processes, namely, a direct process and a water-transfer process. We elucidate the influence of the production process on the microstructural properties of the CNF, as well as the final electrochemical performance. We show that a change in morphology due to capillary forces doubles the specific capacitance of the wet-transferred CNF electrodes.

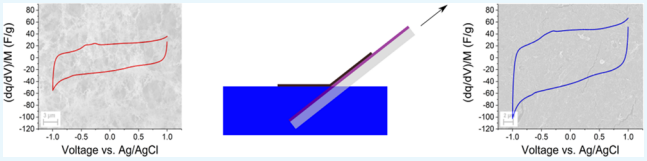

INTRODUCTION

Supercapacitors are electrochemical-energy-storage devices that have gained significant attraction in recent years. They have much promise owing to fast charge times typically associated with dielectric capacitors (in the seconds), coupled with high energy densities normally associated with conventional electrochemical batteries. This is achieved through the formation of an electrical double layer at the interface between the high-surface-area electrodes and an interacting electrolyte.

Carbon nanomaterials, in particular, are well suited to supercapacitor applications.[1,2] Many allotropes have high electrical conductivities, as well as high specific surface areas, making them ideal electrode materials. Moreover, their high porosity allows greater ion displacement from the electrolyte, greatly enhancing the electrical double-layer capacitance responsible for the overall performance of the device.[3] Multiple carbon nanomaterials have been investigated for use in supercapacitor electrodes, including carbon nanotubes, pristine graphene, and reduced graphene oxide (GO). These materials are highly structured and require significant processing to achieve porous structures that maximize the available electrode surface area. An alternative class of materials are carbon foams, which are volumetric, amorphous, and highly porous.[4,5] The morphologies vary depending on the synthesis method, but all varieties of carbon foam have a very high specific surface area up to 1500 m^2/g.[4] In previous studies, supercapacitor electrodes based on carbon foams have achieved specific capacitance up to 330 F/g in aqueous electrolytes, which is highly competitive with other carbon nanomaterials (typically between 50 and 370 F/g).[1,6−10]

Carbon nanofoams (CNFs) are a further subclass of carbon foam formed during the interaction of laser radiation and a carbon-based target.[11−14] The surface morphology of CNFs varies significantly compared to other carbon foams as it is formed in a diffusion-limited aggregation manner rather than by increasing the volume of a bulk precursor.[14] The CNF consists of a significant amount of sp^2 bonds, making the material conductive.[11−13] Among the drawbacks of the CNF are poor mechanical stability and poor substrate adhesion. Although both factors prevent the use of CNF electrodes in aqueous electrolytes, they are stable in many organic electrolyte systems. This has advantages as while aqueous electrolytes offer low cost and ease of processing, organic electrolytes allow for a wider potential window and consequently a higher energy density.[15]

During the preparation of CNFs, the substrate adhesion is low enough that the contact with water is able to delaminate the materials. Interestingly, this phenomenon can be used as a route to transfer the electrode material from an initial substrate to a target by a water-transfer process. In this way, the CNF floats on the top of the water subphase and can subsequently be picked up by withdrawing a submerged substrate from below. While the material is trapped at the air−water interface, morphological changes can occur because of capillary forces. This effect is particularly apparent in materials with a small

Received: August 21, 2018
Accepted: October 29, 2018
Published: November 8, 2018

DOI: 10.1021/acsomega.8b02118
ACS Omega 2018, 3, 15134−15139

characteristic pore size because of the enhancement of the capillary interaction.[16]

In this paper, we demonstrate the preparation and characterization of a CNF-based supercapacitor electrode material through laser processing of a graphene oxide (GO) target. The prepared CNF is transferred onto an appropriate substrate by use of a water-transfer process resulting in a change in the morphology of the foam, which enhances the specific capacitance of the resulting electrodes by a factor of 2. Using Raman spectroscopy, we relate the electrochemical performance enhancement to compression from the capillary forces during the film transfer.

RESULTS AND DISCUSSION

Figure 1 shows the GO characterization used as a precursor for the CNF. Raman spectroscopy shows well-defined D and G

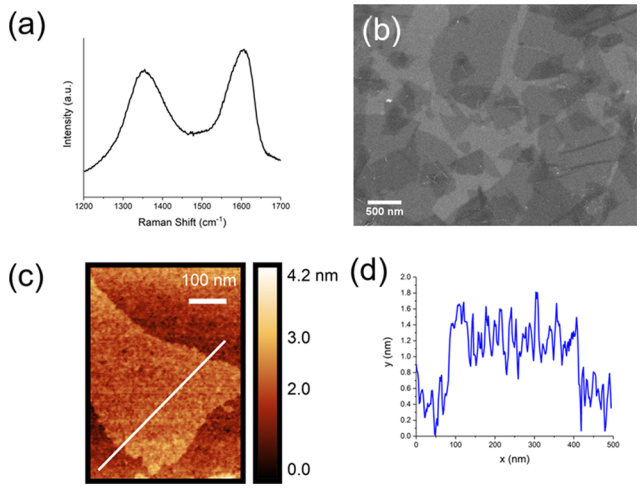

Figure 1. Characterization of prepared GO: (a) Raman peaks, (b) scanning electron microscopy (SEM) image to determine the flake size, (c) atomic force microscopy (AFM) topography, and (d) thickness measurement of the prepared flake.

peaks of the prepared graphene oxide. The flake size of the synthesized GO was between 500 nm and several μm. The flake thickness was 0.8 nm.

Schematics of two fabrication processes to produce CNF on tin-doped indium oxide (ITO) substrates are shown in Figure 2. Figure 2a illustrates the direct deposition approach, where the laser is scanned through an ITO-coated substrate above the GO target. The very first line ablates a small track into the ITO, through which the laser passes afterwards to hit the target. The laser focus is kept on the substrate. The carbon clusters diffuse out of the laser-formed plasma on the target during the reduction of the GO and deposit on the substrate above. Multiple passes form a thick layer of CNF. Since this process involves the formation of a carbon plasma, we are able to prepare CNF with any high-carbon-content material and the feedstock is not limited to GO.

The water-transfer deposition approach is shown in Figure 2b. The glass substrate is immersed in a water bath, whereby the CNF detaches and floats on the water surface as it is less dense than water. The cohesion of the foam is strong enough so it does not break apart when immersed. The CNF is then picked up using an ITO substrate, immersed in the water, and withdrawn at a shallow angle to the water surface.

Imaging by scanning electron microscopy (SEM) (Figure 3) shows a significant difference in morphology between the two deposition methods. The direct-deposited CNF in Figure 3a has a low-density, high-porosity structure with a weblike microstructure. This morphology is typical for a diffusion-limited aggregation formation process.[17] The magnified image in Figure 3b reveals the porous microstructure formed by the clusters, which are then spun into a "web" like appearance. The volumetric character of the CNF did not allow further magnification without charging effects.

The water-transferred sample (Figure 3c) appears to be much denser, where the very fine microstructure of the as-formed CNF has seemingly collapsed, even though the larger-scale porosity appears to be preserved (Figure 3d). The water transfer increases the CNF's conductivity by more than 3 orders of magnitude to 740 μS/m from 360 nS/m.

Sets of electrodes prepared by the two methods described in Figure 2 were used to perform electrochemical measurements. Figure 4a shows cyclic voltammetry (CV) analysis of the CNF prepared by direct deposition onto ITO, as well as of water-transferred films. In both cases, the scan rate was 50 mV/s. All samples exhibit a near-ideal box like CV character. The two visible peaks at around −0.3 V originate from the ITO substrate. Figure 4b shows the scan rate dependence of a water-transferred sample. It is evident that the capacitance falls with the increased scan rate; however, it remains constant up to 100 mV/s scan rate. The box like shape is maintained at all of the scan rates.

Figure 4c illustrates the scan rate dependence of the specific capacitance for the samples shown in Figure 4a. The direct-deposited CNF shows the lower specific capacitance of around 17.5 F/g, while the water-transferred electrode gives a value of 42 F/g. We see immediately that the specific capacitance of the water-transferred CNF is more than double the value of the direct-deposited material. The impedance plot in Figure 4d shows the characteristic steep slope for all of the electrodes at lower frequencies. The ITO substrate is plotted as a reference showing the active material behaving as a supercapacitor.

The cyclic voltammetry measurements of Figure 4a,b show rectangular behavior for the different samples, suggesting an ideal propagation of charges within the electrodes.[18]

The rectangular shape of Figure 4b is maintained up to 100 mV/s scan rate with little variation of the capacitance. The specific capacitance decreases at higher scan rates because ion mobility and the substrate's resistance limit charge separation in the electrolyte.[19] The carbon maintains the rectangular shape at high scan rates, showing good capacitive behavior. The specific capacitance of the direct-deposited values measured for the materials presented are comparable with the work done on CNF systems created in a pulsed laser deposition process.[15]

The results of spectroscopic impedance measurements plotted in Figure 4d highlight the quality of the CNF supercapacitor electrodes prepared here. The steeper the angle at low frequencies, indicating non-diffusion-limited accumulation of electrode surface charge, the closer the system behavior to that of an ideal supercapacitor.[20] The region exhibiting a 45° angle to the axes is characteristic of Warburg behavior (see the inset in Figure 4d), which represents the frequency range where ion diffusion within the electrodes limits the capacitance achievable. A greater Warburg region indicates that the electrode structure is inhibiting the diffusion of electrolyte ions.[18] The Warburg region in these devices is

DOI: 10.1021/acsomega.8b02118
ACS Omega 2018, 3, 15134−15139

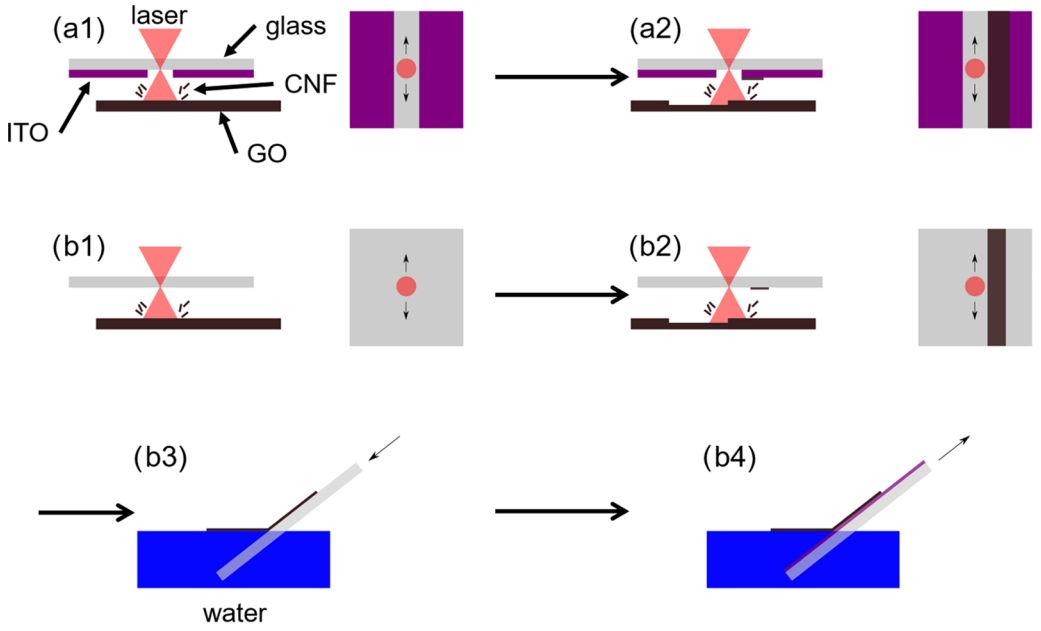

Figure 2. Fabrication schematics of CNF samples: (a1) ITO on glass is held above the GO target, through which the laser is scanned (using a prepatterned slit in the ITO layer). (a2) A thick layer of CNF is deposited on the ITO by moving the GO target to feed the deposition process. (b1) and (b2) show the same deposition process, except a glass substrate is used. (b3) Glass substrate is immersed in water to detach the CNF. (b4) CNF is transferred to the final ITO substrate through a reverse process to (b3).

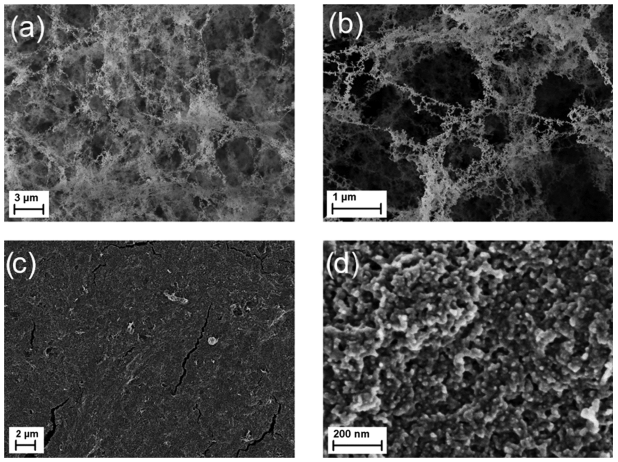

Figure 3. (a) SEM images of CNF directly deposited on ITO. (b) Magnified image of CNF directly deposited on ITO. (c) CNF on ITO after the water-transfer process of Figure 1b. (d) High-magnification image of water-transferred CNF.

smaller for the water-transferred samples than for the direct-deposited ones, showing that the pores are easily accessible for diffusing ions. The intersection with the *x*-axis presents the solution and electrode resistance. The differences lie in the fact that the substrate width was slightly different in all of the measurements. The sample with a smaller width showed a higher intersection value.

The increase of specific capacitance between the direct-deposited CNF and the water-transferred CNF is due to the change in morphology, which we believe is induced by capillary forces during the film transfer.[16] The water transfer creates a different porous structure for ion interaction, which results in an increased system capacitance.[21,22] Porosity is a key parameter in supercapacitor structures as the electric double layer is influenced by the distribution between macro- (>50 nm), meso- (2−50 nm), and micropores (0.7−2 nm). Macro- and mesopores enable good diffusion of ions into the micropores where the surface area is greatly enhanced to accommodate the ions, whereas solvent molecules penetrate only as far as the mesopores.[21] Besides the porosity, the film becomes denser, therefore increasing the electrical contact among the carbon clusters, which increases the conductivity and the specific capacitance.

To investigate the influence of the water transfer on the CNF microstructure further, we turn to Raman spectroscopy. This technique is able to highlight differences in the bonding character as well as doping or strain in carbon nanomaterials.[23−27] Raman spectra of the CNF directly deposited on a glass substrate and a CNF sample water transferred from a glass substrate onto a glass substrate are shown in Figure 5. The spectra are stacked and normalized to the G-peak intensity for comparison.

We note several changes to the Raman spectra of the water-transferred material, when compared to the direct-deposited CNF. All three peaks show a blue shift of three wavenumbers after the water transfer. In carbon materials, this shift to lower wavenumbers is associated with a mechanical deformation in the material.[23,28−30] The $I(D)/I(G)$ ratio increases after the water transfer. This is an indication that the disorder in the carbon increases.[31] The shift of the D′-peak is another indication that the disorder in the material is increasing.[32] The peak showing up at around 1100 cm^{-1} originates in the underlying borosilicate glass substrate.

The increase of specific capacitance is not only from the change in morphology but the capillary forces also introduce stress into the material. During the water transfer, the water enters the porous CNF and capillary forces start compressing the film. This not only changes the surface structure but also induces a compressive stress into the carbon. It is known that compressive forces can enhance the specific capacitance of carbon films.[33] The enhanced specific capacitance therefore

DOI: 10.1021/acsomega.8b02118
ACS Omega 2018, 3, 15134−15139

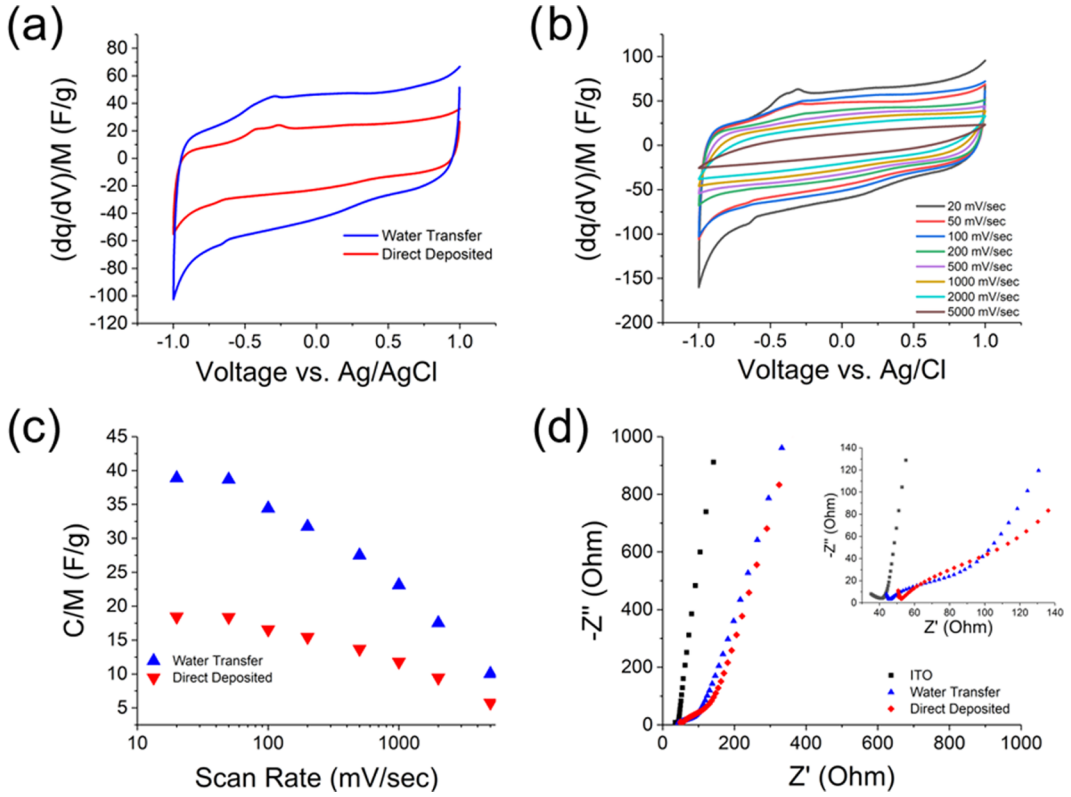

Figure 4. (a) CV scans of the two different CNF electrode materials at 50 mV/s scan rate. (b) Scan rate dependence of the water-transferred electrode material. (c) Specific capacitance of the two samples as a function of scan rate. (d) Nyquist plot of spectroscopic impedance measurements of the electrode materials, showing the blank ITO substrate as a reference; the inset shows the low-impedance region.

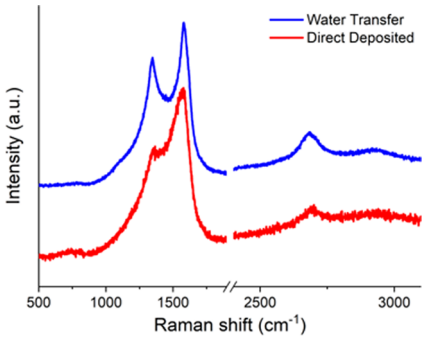

Figure 5. Raman spectra of direct-deposited and water-transferred CNFs onto a glass substrate.

originates from two different components, namely, a change in morphology, making a more dense film as well as the pores more accessible, and a compressive stress induced by the capillary forces, which increases the capacitance further.

CONCLUSIONS

We have demonstrated the preparation and characterization of a carbon-nanofoam-based supercapacitor electrode material. The material is prepared through infrared laser treatment of a graphene oxide target, and may be directly deposited onto a current collector layer (in this case ITO), or may be transferred from a glass substrate using a water-transfer process. We observe significant changes to the morphology of the CNF when transferred in this fashion, including the development of compressive stress (as characterized using Raman spectroscopy). This effect arises because of the influence of capillary forces during the transfer process. The outcome is a significant increase in the specific capacitance of the CNF, from 17.5 F/g to around 42 F/g.

METHODS

Graphene oxide was prepared using the Hummers method.[34,35] The GO was characterized using atomic force microscopy to determine the flake thickness, SEM to characterize the flake size, and Raman spectroscopy. For characterization, the GO was spin-coated onto a silicon substrate. The GO was deposited by drop-casting onto a borosilicate glass slide. The glass slide was completely covered and left to dry at 50 °C to hasten the drying process. A second drop-casting step was added to create a thick layer of GO on the glass slide; it was again left to dry at 50 °C. The film thickness was aimed to be more than 200 μm. The GO target was put in an oven and heated up to 250° in a ramp process for 1.5 h and then left at room temperature to cool down.

The exact experimental setup to create the CNF is described elsewhere.[17] A brief summary is as follows: the targets were irradiated with a Multiwave Nd:YAG nanosecond pulsed infrared laser (set at 10 ns) in ambient conditions with a set fluence of 417 mJ/cm^2. To form the CNF on the substrate, it was held stationary over the target with a small (<1 mm) air gap in between, allowing the aggregation of the carbon clusters on the substrate.

The weight of the CNF was measured using a Mettler Toledo microbalance. Six lines were deposited onto the same substrate to get weight well outside of the error of the balance. The substrates were measured before and after the deposition.

DOI: 10.1021/acsomega.8b02118
ACS Omega 2018, 3, 15134−15139

The measured weight was then divided by the number of lines deposited.

Samples were imaged with a Zeiss SIGMA field emission gun scanning electron microscope (FEG-SEM) using a Zeiss in-lens secondary electron detector. The FEG-SEM working conditions used were as follows: 1 kV accelerating voltage, 20 μm aperture, and 2 mm working distance.

Electrochemical measurements were performed with a 3-electrode configuration using a Gamry 600+ reference potentiostat. The counter electrode was a platinum wire, and the reference electrode was silver/silver chloride (Ag/AgCl). The electrolyte used was 0.1 M lithium perchlorate ($LiClO_4$) in acetonitrile. Cyclic voltammetry measurements were performed in a range of −1 to +1 V versus Ag/AgCl for a variety of scan rates from 20 to 5000 mV/s. Impedance spectroscopy applied a perturbation signal of 10 mV around 0 V at frequencies from 100 kHz to 0.1 Hz.

Raman measurements were carried out using a Renishaw Invia Microscope. A 532 nm 50 mW continuous wave laser was used at 10% intensity for 10 s to produce the Raman spectrum. A total of 10 accumulations were used to enhance the signal.

A Bruker Dimension Icon atomic force microscope (AFM) was used in peak force mode to measure the thickness of the GO flakes.

AUTHOR INFORMATION

Corresponding Authors

*E-mail: sebastian.nufer@m-solv.com (S.N.).
*E-mail: A.B.Dalton@sussex.ac.uk (A.B.D.).

ORCID

Sebastian Nufer: 0000-0003-2636-8738
Peter Lynch: 0000-0001-8805-0632
Matthew J. Large: 0000-0001-7295-7619
Sandra Víctor-Román: 0000-0003-0924-5840
Ana M. Benito: 0000-0002-8654-7386
Wolfgang K. Maser: 0000-0003-4253-0758

Notes

The authors declare no competing financial interest.

ACKNOWLEDGMENTS

This work has received funding from the European Union's Horizon 2020 research and innovation programme under the Marie Skłodowska-Curie grant agreement no. 642742. A.M.B., J.H.-F., and W.K.M. acknowledge Spanish MINEICO (project ENE2016-79282-C5-1-R), the Gobierno de Aragón (Grupo Reconocido DGA-T03_17R), and associated EU Regional Development Funds. S.V.-R. thanks Spanish MINEICO for her Ph.D. grant (BES2014-068727 and associated EU Social Funds).

REFERENCES

(1) Zhang, L. L.; Zhao, X. Carbon-Based Materials as Supercapacitor Electrodes. *Chem. Soc. Rev.* **2009**, *38*, 2520−2531.
(2) González, A.; Goikolea, E.; Barrena, J. A.; Mysyk, R. Review on Supercapacitors: Technologies and Materials. *Renewable Sustainable Energy Rev.* **2016**, *58*, 1189−1206.
(3) Frackowiak, E.; Beguin, F. Carbon Materials for the Electrochemical Storage of Energy in Capacitors. *Carbon* **2001**, *39*, 937−950.
(4) Inagaki, M.; Qiu, J.; Guo, Q. Carbon Foam: Preparation and Application. *Carbon* **2015**, *87*, 128−152.
(5) Chen, C.; Kennel, E. B.; Stiller, A. H.; Stansberry, P. G.; Zondlo, J. W. Carbon Foam Derived from Various Precursors. *Carbon* **2006**, *44*, 1535−1543.
(6) Chen, J.; Xu, J.; Zhou, S.; Zhao, N.; Wong, C.-P. Nitrogen-Doped Hierarchically Porous Carbon Foam: A Free-Standing Electrode and Mechanical Support for High-Performance Supercapacitors. *Nano Energy* **2016**, *25*, 193−202.
(7) Fan, Z.; Qi, D.; Xiao, Y.; Yan, J.; Wei, T. One-Step Synthesis of Biomass-Derived Porous Carbon Foam for High Performance Supercapacitors. *Mater. Lett.* **2013**, *101*, 29−32.
(8) Sawant, S. Y.; Han, T. H.; Ansari, S. A.; Shim, J. H.; Nguyen, A. T. N.; Shim, J.-J.; Cho, M. H. A Metal-Free and Non-Precious Multifunctional 3D Carbon Foam for High-Energy Density Supercapacitors and Enhanced Power Generation in Microbial Fuel Cells. *J. Ind. Eng. Chem.* **2018**, *60*, 431−440.
(9) Xin, Z.; Fang, W.; Zhao, L.; Chen, H.; He, X.; Zhang, W. N-Doped Carbon Foam Constructed by Liquid Foam with Hierarchical Porous Structure for Supercapacitor. *J. Porous Mater.* **2018**, *25*, 1521−1529.
(10) Zhang, X.; Zhao, J.; He, X.; Li, Q.; Ao, C.; Xia, T.; Zhang, W.; Lu, C.; Deng, Y. Mechanically Robust and Highly Compressible Electrochemical Supercapacitors from Nitrogen-Doped Carbon Aerogels. *Carbon* **2018**, *127*, 236−244.
(11) Rode, A. V.; Hyde, S.; Gamaly, E.; Elliman, R.; McKenzie, D.; Bulcock, S. Structural Analysis of a Carbon Foam Formed by High Pulse-Rate Laser Ablation. *Appl. Phys. A: Mater. Sci. Process.* **1999**, *69*, S755−S758.
(12) Rode, A. V.; Gamaly, E. G.; Luther-Davies, B. Formation of Cluster-Assembled Carbon Nano-Foam by High-Repetition-Rate Laser Ablation. *Appl. Phys. A: Mater. Sci. Process.* **2000**, *70*, 135−144.
(13) Muñoz, E.; de Val, M.; Ruiz-González, M. L.; López-Gascón, C.; Sanjuán, M. L.; Martinez, M. T.; González-Calbet, J. M.; Germán, F.; Laguna, M. Gold/carbon Nanocomposite Foam. *Chem. Phys. Lett.* **2006**, *420*, 86−89.
(14) Henley, S.; Carey, J.; Silva, S.; Fuge, G.; Ashfold, M.; Anglos, D. Dynamics of Confined Plumes during Short and Ultrashort Pulsed Laser Ablation of Graphite. *Phys. Rev. B* **2005**, *72*, No. 205413.
(15) Spanakis, E.; Pervolaraki, M.; Giapintzakis, J.; Katsarakis, N.; Koudoumas, E.; Vernardou, D. Effect of Gold and Silver Nanoislands on the Electrochemical Properties of Carbon Nanofoam. *Electrochim. Acta* **2013**, *111*, 305−313.
(16) Whitten, P. G.; Spinks, G. M.; Wallace, G. G. Mechanical Properties of Carbon Nanotube Paper in Ionic Liquid and Aqueous Electrolytes. *Carbon* **2005**, *43*, 1891−1896.
(17) Nufer, S.; Fantanas, D.; Ogilvie, S. P.; Large, M. J.; Winterauer, D. J.; Salvage, J. P.; Meloni, M.; King, A. A.; Schellenberger, P.; Shmeliov, A.; et al. Percolating Metallic Structures Templated on Laser-Deposited Carbon Nanofoams Derived from Graphene Oxide: Applications in Humidity Sensing. *ACS Appl. Nano Mater.* **2018**, *1*, 1828−1835.
(18) Stoller, M. D.; Park, S.; Zhu, Y.; An, J.; Ruoff, R. S. Graphene-Based Ultracapacitors. *Nano Lett.* **2008**, *8*, 3498−3502.
(19) Lota, G.; Centeno, T. A.; Frackowiak, E.; Stoeckli, F. Improvement of the Structural and Chemical Properties of a Commercial Activated Carbon for Its Application in Electrochemical Capacitors. *Electrochim. Acta* **2008**, *53*, 2210−2216.
(20) Kim, M.; Oh, I.; Kim, J. Effects of Different Electrolytes on the Electrochemical and Dynamic Behavior of Electric Double Layer Capacitors Based on a Porous Silicon Carbide Electrode. *Phys. Chem. Chem. Phys.* **2015**, *17*, 16367−16374.
(21) Borchardt, L.; Oschatz, M.; Kaskel, S. Tailoring Porosity in Carbon Materials for Supercapacitor Applications. *Mater. Horiz.* **2014**, *1*, 157−168.
(22) Rose, M.; Korenblit, Y.; Kockrick, E.; Borchardt, L.; Oschatz, M.; Kaskel, S.; Yushin, G. Hierarchical Micro-and Mesoporous Carbide-Derived Carbon as a High-Performance Electrode Material in Supercapacitors. *Small* **2011**, *7*, 1108−1117.

DOI: 10.1021/acsomega.8b02118
ACS Omega 2018, 3, 15134−15139

(23) Ni, Z. H.; Yu, T.; Lu, Y. H.; Wang, Y. Y.; Feng, Y. P.; Shen, Z. X. Uniaxial Strain on Graphene: Raman Spectroscopy Study and Band-Gap Opening. *ACS Nano* **2008**, *2*, 2301−2305.
(24) Das, A.; Pisana, S.; Chakraborty, B.; Piscanec, S.; Saha, S.; Waghmare, U.; Novoselov, K.; Krishnamurthy, H.; Geim, A.; Ferrari, A.; et al. Monitoring Dopants by Raman Scattering in an Electrochemically Top-Gated Graphene Transistor. *Nat. Nanotechnol.* **2008**, *3*, 210−215.
(25) Kim, S.; Park, S.; Kim, H.; Jang, G.; Park, D.; Park, J.-Y.; Lee, S.; Ahn, Y. Characterization of Chemical Doping of Graphene by in-Situ Raman Spectroscopy. *Appl. Phys. Lett.* **2016**, *108*, No. 203111.
(26) Ferrari, A.; Robertson, J. Resonant Raman Spectroscopy of Disordered, Amorphous, and Diamondlike Carbon. *Phys. Rev. B* **2001**, *64*, No. 075414.
(27) Cronin, S. B.; Swan, A.; Ünlü, M.; Goldberg, B.; Dresselhaus, M.; Tinkham, M. Measuring the Uniaxial Strain of Individual Single-Wall Carbon Nanotubes: Resonance Raman Spectra of Atomic-Force-Microscope Modified Single-Wall Nanotubes. *Phys. Rev. Lett.* **2004**, *93*, No. 167401.
(28) Huang, M.; Yan, H.; Heinz, T. F.; Hone, J. Probing Strain-Induced Electronic Structure Change in Graphene by Raman Spectroscopy. *Nano Lett.* **2010**, *10*, 4074−4079.
(29) Liu, Z.; Zhang, J.; Gao, B. Raman Spectroscopy of Strained Single-Walled Carbon Nanotubes. *Chem. Commun.* **2009**, 6902−6918.
(30) Sakata, H.; Dresselhaus, G.; Dresselhaus, M.; Endo, M. Effect of Uniaxial Stress on the Raman Spectra of Graphite Fibers. *J. Appl. Phys.* **1988**, *63*, 2769−2772.
(31) Jorio, A.; Ferreira, E. H. M.; Cançado, L. G.; Achete, C. A.; Capaz, R. B. Measuring Disorder in Graphene with Raman Spectroscopy. In *Physics and Applications of Graphene-Experiments*; InTech, 2011.
(32) Zhang, G.; Sun, S.; Yang, D.; Dodelet, J.-P.; Sacher, E. The Surface Analytical Characterization of Carbon Fibers Functionalized by H2SO4/HNO3 Treatment. *Carbon* **2008**, *46*, 196−205.
(33) Li, X.; Rong, J.; Wei, B. Electrochemical Behavior of Single-Walled Carbon Nanotube Supercapacitors under Compressive Stress. *ACS Nano* **2010**, *4*, 6039−6049.
(34) Hummers, W. S., Jr.; Offeman, R. E. Preparation of Graphitic Oxide. *J. Am. Chem. Soc.* **1958**, *80*, 1339.
(35) Vallés, C.; Núñez, J. D.; Benito, A. M.; Maser, W. K. Flexible Conductive Graphene Paper Obtained by Direct and Gentle Annealing of Graphene Oxide Paper. *Carbon* **2012**, *50*, 835−844.

DOI: 10.1021/acsomega.8b02118
ACS Omega 2018, 3, 15134−15139